Stem Cell Reviews and Reports (2023) 19:2837–2851
https://doi.org/10.1007/s12015-023-10600-7

Dbx2, an Aging-Related Homeobox Gene, Inhibits the Proliferation of Adult Neural Progenitors

Andrea Giuliani[1] · Valerio Licursi[2] · Paola S. Nisi[1] · Mario Fiore[2] · Sara D'Angelo[1] · Stefano Biagioni[1] · Rodolfo Negri[1,2] · Peter J. Rugg-Gunn[3,4] · Emanuele Cacci[1] · Giuseppe Lupo[1]

Accepted: 19 July 2023 / Published online: 22 August 2023

Abstract

In the adult mouse brain, the subventricular zone (SVZ) underlying the lateral ventricles harbours a population of quiescent neural stem cells, which can be activated (aNSCs) to initiate proliferation and generate a neurogenic lineage consisting of transit amplifying progenitors (TAPs), neuroblasts (NBs) and newborn neurons. This process is markedly reduced during aging. Recent studies suggest that the aged SVZ niche decreases the pool of proliferating neural/stem progenitor cells (NSPCs), and hence adult neurogenesis, by causing transcriptomic changes that promote NSC quiescence. The transcription factors that mediate these changes, however, remain unclear. We previously found that the homeobox gene *Dbx2* is upregulated in NSPCs of the aged mouse SVZ and can inhibit the growth of NSPC cultures. Here, we further investigate its role as a candidate transcriptional regulator of neurogenic decline. We show that *Dbx2* expression is downregulated by Epidermal Growth Factor receptor signaling, which promotes NSPC proliferation and decreases in the aged SVZ. By means of transgenic NSPC lines overexpressing *Dbx2*, we also show that this gene inhibits NSPC proliferation by hindering the G2/M transition. Furthermore, we exploit RNA sequencing of transgenic NSPCs to elucidate the transcriptomic networks modulated by *Dbx2*. Among the top hits, we report the downregulation of the molecular pathways implicated in cell cycle progression. Accordingly, we find that *Dbx2* function is negatively correlated with the transcriptional signatures of proliferative NSPCs (aNSCs, TAPs and early NBs). These results point to Dbx2 as a transcription factor relaying the anti-neurogenic input of the aged niche to the NSPC transcriptome.

Keywords Adult neurogenesis · Neural stem/progenitor cells · Subventricular zone · Transcriptional regulation · Cell cycle

Introduction

In adult mice, the subventricular zone (SVZ) of the lateral ventricles and the subgranular zone (SGZ) of the dentate gyrus harbour neurogenic neural stem/progenitor cells (NSPCs) within a specialized niche. The niche milieu includes other cell types, such as ependymal, vascular, glial and neuronal cells, as well as locally produced cues and systemic factors, acting together to support NSPC maintenance and neuronal differentiation [1]. SVZ and SGZ NSPCs are organized in a hierarchical cell lineage encompassing the neurogenic process [2, 3]. Neural stem cells (NSCs) lie at the top of the lineage and are largely quiescent (qNSCs). Upon activation (aNSCs) by appropriate stimuli, they can enter the cell cycle, to self-renew or to generate daughter cells that give rise to transient amplifying progenitors (TAPs), neuroblasts (NBs) and newborn neurons [4, 5].

Andrea Giuliani and Valerio Licursi contributed equally to this work.

✉ Valerio Licursi
valerio.licursi@uniroma1.it

✉ Giuseppe Lupo
giuseppe.lupo@uniroma1.it

1 Department of Biology and Biotechnologies Charles Darwin, Sapienza University of Rome, 00185 Rome, Italy

2 Institute of Molecular Biology and Pathology (IBPM), National Research Council (CNR), Rome, Italy

3 Epigenetics Programme, The Babraham Institute, Cambridge CB22 3AT, UK

4 Wellcome Trust – Medical Research Council Cambridge Stem Cell Institute, University of Cambridge, Cambridge CB2 1QR, UK

An age-related reduction of adult neurogenesis might be a contributing factor to the cognitive decline of elderly humans [6, 7]. This is best documented in mice, wherein proliferating NSPCs and their neuronal output are markedly decreased in the aged SVZ and SGZ [8, 9]. Two explanations have been proposed for this reduction. Earlier models suggest that the age-dependent decrease in neurogenesis is driven by the progressive exhaustion of the qNSC pool due to their activation and differentiation [10, 11]. According to recent studies, however, a qNSC reservoir persists in the aged brain [12–15]. Moreover, some NSCs may return to quiescence after activation and self-renewal [16–18]. These observations lead to alternative models, whereby the neurogenic decline may be caused by the increased quiescence of the aged NSC pool. Considering the heterogeneous nature of NSC populations [12, 14, 15], and the time-dependent changes in neurogenesis [16, 19], both models may be represented in certain NSC subpopulations and/or ages.

Adult NSPC proliferation is influenced by various extracellular signals. In the mouse SVZ, Epidermal Growth Factor receptor (EGFR) signaling is crucial to NSC activation, and is reduced in qNSCs and in the aged niche [20–23]. In contrast, inflammatory pathways, such as interferon (IFN) signaling, increase in the aged SVZ and promote NSC quiescence [14, 24]. Tumor Necrosis Factor α (TNFα), Transforming Growth Factor β (TGFβ) and Fibroblast Growth Factor (FGF) pathways are also implicated in NSC activation and aging [18, 25–27].

Transcriptomic comparison of qNSCs and aNSCs has revealed clear differences in the expression of genes related to cell cycle, protein synthesis and inflammatory response [16, 18, 22]. Transcriptomic changes have also been detected between young adult and aged NSPCs [12, 14, 15, 28–30]. This suggests that transcriptional regulation in NSPCs is key to control their proliferation and to the alterations of aged NSPCs. It is therefore important to identify the transcription factors that relay aged niche signals to the NSPC transcriptome and uncover how they function in this context.

The homeobox gene *Dbx2* encodes a transcription factor involved in the development of spinal cord interneurons, and is also expressed in selected regions of the embryonic brain, limb buds and tooth germs [31, 32]. We previously reported that *Dbx2* is expressed in the adult mouse SVZ, and established that *Dbx2* is upregulated in aged NSPCs and inhibits the growth of NSPC cultures [30]; however, the extracellular signals controlling *Dbx2* expression and the mechanisms mediating *Dbx2* function remained unclear. Here, we show that *Dbx2* transcription is negatively modulated by EGFR signaling. We provide evidence that *Dbx2* can hinder the G2/M transition in adult NSPCs, thus reducing their proliferation. Finally, we describe the *Dbx2*-regulated transcriptome in adult NSPC cultures. Notably, this expression program includes cell cycle and inflammatory response gene networks, and is negatively correlated with the signatures of the proliferative neurogenic cell types (aNSCs, TAPs and early NBs).

Materials and Methods

NSPC Culture

This work was carried out by *in vitro* culture of mouse NSPCs that were previously derived from the SVZ of young adult (3 months old, 3 mo) C57BL/6 J/Babr mice [30]. NSPC culture in adherent and non-adherent proliferative conditions was performed according to published protocols [30, 33, 34]. Briefly, NSPCs were seeded in T25 flasks or 6-well plates coated with poly-ornithine (Sigma-Aldrich P3655, 10 μg/ml) and laminin (Sigma-Aldrich L2020, 5 μg/ml) for adherent cultures, or non-coated T25 flasks for non-adherent conditions. In both cases, NSPCs were cultured with DMEM/F12 (Invitrogen 32500035), supplemented with GlutaMAX (Invitrogen 35050038, 1:100), HEPES (Sigma-Aldrich H0887, 5 mM), sodium bicarbonate (Sigma-Aldrich S8761, 11.25 mg/ml), D-glucose (Sigma Aldrich G8769, 0.6%), B27 supplement (Invitrogen 17504044, 1:50), human recombinant EGF (R&D Systems 236-EG-200/CF, 20 ng/ml) and FGF2 (R&D Systems 233-FB-25/CF, 10 ng/ml). Non-adherent cultures were also supplemented with heparin (Sigma-Aldrich, H3149, 2 μg/ml). Transgenic NSPC lines with constitutive expression of a *Dbx2* transgene or a control *GFP* transgene were previously described [30]. Briefly, NSPC transfection of young adult SVZ NSPCs with *pTP6-hrGFP* or *pTP6-Dbx2* plasmids was previously carried out using an Amaxa mouse NSC Nucleofector kit (Lonza VPG-1004) on an Amaxa Nucleofector II (Lonza), followed by selection and maintenance of transgenic NSPCs by treatment with puromycin (Sigma-Aldrich P8833, 1 μg/ml). Two different pairs of transgenic NSPC lines were previously generated from independent derivations of young adult mouse SVZ NSPCs, and were used again for this work. All the experiments reported in this study were performed with NSPCs bulk-cultured for up to 24 passages *in vitro* starting from the primary culture of dissociated SVZ cells (passage 1).

Real-time qRT-PCR Assays

For the analysis of *Dbx2* mRNA levels by real-time qRT-PCR, young adult SVZ NSPCs were seeded in T25 flasks or 6-well plates at a density of approximately 40000 cells/cm^2 in adherent proliferative culture conditions. On the next day, cultures were rinsed once with medium devoid of EGF and FGF2, then incubated in fresh medium with both EGF and FGF2, none of them, or only one of them. Treatments with human recombinant Transforming Growth Factor α (TGFα, Cell Guidance Systems GFH39-5) were performed by diluting a 50 µg/ml stock in PBS containing 0.1% Bovine Serum Albumin with culture medium to 100 ng/ml. Treatments with the EGFR inhibitor AG1478 (Calbiochem 658548) were performed by diluting a 10 mM stock in DMSO with culture medium to 2 µM; control cultures were treated with equal volumes of DMSO. At the end of the experimental treatment, cells cultured in T25 flasks were enzymatically detached with Accutase (Corning 25–058-CI), pelleted in 2 ml tubes and lysed for RNA purification, whereas cells in 6-well plates were directly lysed in the culture plates. Total RNA purification and quantification, reverse transcription and real-time qPCR were performed using Qiagen kits, a NanoDrop 2000 (Thermo Scientific) and a Rotor-Gene Q (Qiagen), as previously described [33]. The following primers were used for *Dbx2* and for the reference gene *Rpl19*: *Dbx2*_forward CCCGCCATTCTACTCTGCAT, *Dbx2*_reverse GAGTCCTGGGTCAGCAAAGG, *Rpl19*_forward AGACCAAGGAAGCACGAAAG, *Rpl19*_reverse GCCGCTATGTACAGACACGA.

Cell Proliferation Analyses by Flow Cytometry and Immunocytochemistry

For cell cycle analysis, transgenic NSPCs were seeded in T25 flasks at a density of 5000 cells/cm^2 in non-adherent culture conditions supplemented with 600 ng/ml of puromycin. Neurospheres generated by control or *Dbx2*-overexpressing NSPCs were pelleted by centrifugation and dissociated with Accutase. The resulting cell suspensions were rinsed with PBS, fixed in cold PBS-methanol 1:1 and stored in this solution at 4 °C. Staining with propidium iodide (PI) and quantification of the fraction of cells in G0/G1, S and G2/M by flow cytometry were performed as previously described [35].

To quantify the fraction of cells expressing Ki67 and phosphorylated histone H3 (pH3), control and *Dbx2*-overexpressing neurospheres were collected by centrifugation and dissociated, followed by cell plating on poly-ornithine/laminin coated glass coverslips in 24-well plates and culture for 2-4 hours (2–4 h) in media for adherent proliferative conditions to allow attachment to the glass. After attachment, cells were fixed for 20 min with methanol-free formaldehyde (Pierce 28908) diluted to 4% with PBS, then rinsed a few times with PBS and stored in PBS at 4 °C. Immunofluorescence analysis with an anti-Ki67 mouse monoclonal antibody (Leica Biosystems ACK02, 1:100) or with an anti-pH3 (Ser 10) rabbit polyclonal antibody (ThermoFisher PA5-17869, 1:100) was performed as previously described [30, 35]. In each experiment, 12 random fields per coverslip were selected based on Hoechst staining and photographed using a Nikon Eclipse TE300 microscope and a Nikon DS-U3 digital camera, followed by the quantification of the ratio between Ki67-positive (Ki67+) or pH3-positive (pH3+) cells and the total cell number in 1–3 coverslips for each experimental condition. Several hundred to a few thousand cells were counted for each condition in each experiment. Automated immunofluorescence analysis was performed with ImageJ software [36]. Colocalization images were generated using the ImageJ plug-in "Colocalization Image Creator" [37]. For Hoechst signal, the "Binary Element" option was used, and the automatic thresholding was set on "YEN"; for Ki67 and pH3 signals, the "Grayscale Element" option was chosen. The colocalization images generated were then used for automated counting of Ki67+ or pH3+ cells using the ImageJ plug-in "Colocalization Object Counter" [37]. Only Ki67 and pH3 signals effectively colocalizing with Hoechst signal were counted. Automated analysis of signal intensity was performed using the ImageJ tool "Analyse Particles". A nuclear mask was generated using Hoechst signal to specifically select nuclear regions. This mask was then merged with the Ki67 or pH3 signals and the fluorescence intensity per pixel in each nucleus was measured with the ImageJ tool "Measure".

Statistical Analysis of Gene Expression and Cell Proliferation Assays

The experimental data obtained from qRT-PCR, flow cytometry and immunofluorescence assays were analysed and graphically represented using GraphPad Prism 9 software. The type of statistical test performed, the resulting *p* values and the number of independent experimental replicates performed with NSPCs from different culture passages (n) are indicated in the figure legends.

RNA-sequencing and Differential Gene Expression Analysis

For RNA-sequencing (RNA-seq), total RNA was purified from frozen cell pellets of control and *Dbx2*-overexpressing non-adherent cultures using Qiagen RNeasy kits. RNA-seq libraries from total RNA (100 ng) from each sample were prepared using QuantSeq 3' mRNA-Seq Library prep kit (Lexogen, Vienna, Austria), according to manufacturer's instructions, at Next Generation Diagnostics (Pozzuoli, Italy). The amplified fragmented cDNAs of 300 bp in size were sequenced in single-end mode using the NextSeq500 (Illumina) with a read length of 101 bp. Sequence read quality was evaluated using *FastQC* version 0.11.8 (Babraham Institute, Cambridge, UK), followed by trimming using *bbduk* software to remove adapter sequences, poly-A tails and low-quality end bases ($Q<20$). Reads were then mapped to the mouse Ensembl GRCm38 (mm10) build reference genome with *STAR* version 2.5.0a [38]; gene annotations corresponding to Ensembl annotation release 96 were used to build a transcriptome index, which was provided to *STAR* during the alignment.

To identify differentially expressed genes (DEGs), data were filtered to remove from the analysis the genes having > 1 counts per million in less than 4 out of 16 total samples. Data normalization and differential gene expression analysis were performed using Bioconductor, R package *edgeR* version 3.36 [39], assigning the cell line batch as a covariate to fit the generalized log-linear model with the glmQLFit function of *edgeR*. DEGs were assessed by comparing *Dbx2*-NSPC and *GFP*-NSPC samples using a moderated t-test with a false discovery rate (FDR) < 0.05 threshold. Volcano plot was created using Bioconductor [40, 41], R package *EnhancedVolcano* version 1.12.0. Principal component analysis (PCA) was performed using R base prcomp function, plotting the first two PCs using R package *ggplot2* version 3.3.5.

Gene Ontology, Gene Set and Transcription Factor Enrichment Analyses

DEGs in *Dbx2*-NSPCs vs *GFP*-NSPCs were clustered by functional annotation in gene ontology (GO) and pathway enrichment analysis using Bioconductor R package *clusterProfiler* version 4.2.0 [42] with annotation of GO database [43], and with annotation of REACTOME [44] and Kyoto Encyclopedia of Genes and Genomes (KEGG) [45] for pathways. R package *pathview* version 1.34.0 was used to integrate the RNA-seq data with KEGG pathway plots.

Broad Institute gene set enrichment analysis (GSEA) [46] was used to assess the enrichment of the *Dbx2*-associated signature list (12533 expressed genes in *Dbx2*-NSPCs and *GFP*-NSPCs without FDR threshold, ranked according to fold change (FC), versus the curated "Hallmark" and "C2" gene set collections from the Broad Molecular Signatures Database (MSigDB) version 7.4.1 (https://www.gsea-msigdb.org/gsea/msigdb/), or versus recently published mouse SVZ single-cell RNA-seq datasets [14, 15, 47]. The mouse version of the gene set collections "Hallmark" and "C2" (REACTOME subcategory, selecting signatures related to cell cycle) were obtained from R package *msigdbr* version 7.4.1. GSEA enrichment score (ES) was calculated by walking down the ranked list of genes, increasing a running-sum statistic when a gene was in the gene set and decreasing it when it was not. A normalized ES (NES) was also calculated with GSEA, by considering differences in pathway size (i.e., gene set size) and allowing for comparisons between pathways within the analysis.

Transcription factor enrichment analysis was performed with Enrichr method [48], using as references TRANSFAC and JASPAR library [49], containing manually curated transcription factors binding profiles as position weight matrices, TRRUST library [50], a database of reference transcription factor-target regulatory interactions, and ENCODE and CHEA library, containing experimental transcription factor binding data from ENCODE Project Consortium [51] and CHEA database [52].

Results

Dbx2 Expression is Upregulated in Aged or Quiescent NSPCs and is Repressed by EGFR Signaling

We previously reported that *Dbx2* mRNA levels were increased both in NSPC cultures and in freshly isolated NSPCs obtained from the SVZ of aged (18 mo) mice as compared to adult (3–7 mo) samples [30]. To confirm these results, we checked a recent transcriptomic dataset of NSPCs isolated from the SVZ of 2 mo, 7 mo and 19 mo mice, noticing an age-dependent upregulation of *Dbx2* [14] (Fig. 1A). We also examined published transcriptomic datasets of qNSCs and aNSCs isolated from the adult mouse SVZ [15, 18, 22], consistently observing *Dbx2* upregulation in qNSCs (Fig. 1B to D).

We then investigated whether EGFR signaling may be involved in *Dbx2* expression changes upon NSC activation or NSPC aging. To this goal, we analysed *Dbx2* mRNA levels in cultures of young adult (3 mo) mouse SVZ NSPCs that were maintained for 6 h in standard proliferation-supporting media, supplemented with EGF and FGF2, in media devoid of both growth factors, or in media containing only EGF or FGF2. As shown in Fig. 1E, *Dbx2* was upregulated in NSPC cultures devoid of exogenous EGF, when compared with EGF-supplemented cultures. Furthermore, *Dbx2* was downregulated when NSPCs were cultured without growth factors for 6 h and then treated with EGF for 2 h, as compared to growth factor withdrawal for 8 h (Fig. 1F). TGFα is the predominant EGFR ligand in the adult brain and its levels decrease in the aged SVZ [21]. We observed a comparable decrease in *Dbx2* mRNA levels in NSPC cultures treated for 6 h with either EGF or TGFα, in comparison with NSPCs cultured without exogenous growth factors; this decrease was prevented by including AG1478, an EGFR inhibitor, in the culture media (Fig. 1G). These results suggest that EGFR signaling represses *Dbx2* expression in SVZ NSPCs; consequently, a reduction of EGFR activation during quiescence or aging may lead to *Dbx2* upregulation in NSPCs (Fig. 1H).

Dbx2 Overexpression in Young Adult Mouse SVZ NSPCs Inhibits Cell Proliferation by Hindering the G2/M Transition

Dbx2 overexpression reduces the growth of NSPC cultures derived from the SVZ of young adult mice, without major effects on NSPC viability, suggesting that *Dbx2* inhibits NSPC

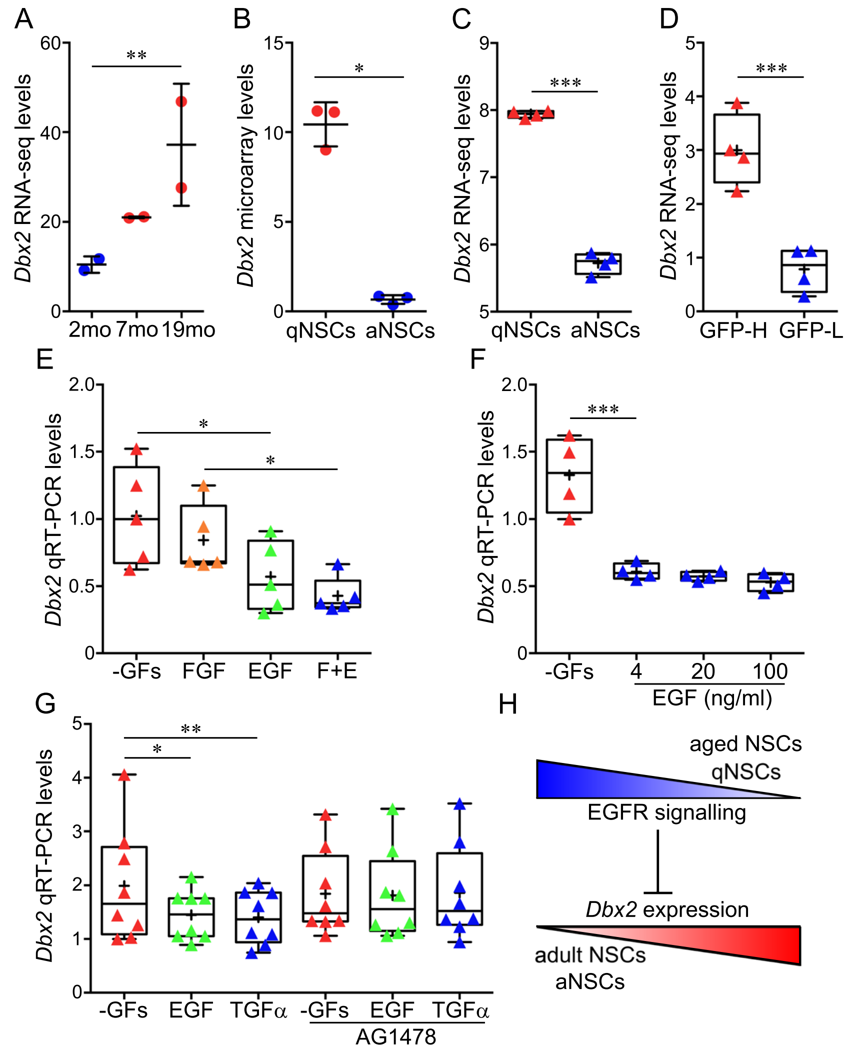

Fig. 1 Activation and EGFR signaling downregulate *Dbx2* expression in adult NSPCs. **(A)** *Dbx2* mRNA levels in freshly isolated NSPCs from the SVZ of 2 mo, 7 mo and 19 mo mice as reported in a published RNA-seq dataset [14]. Black lines show mean transcript levels ± standard deviation; blue and red dots show individual experimental replicates for young adult and aged mice, respectively ($n=2$); **, adjusted p value < 0.01, 2 mo vs 19 mo NSPCs. **(B)** *Dbx2* mRNA levels in freshly isolated qNSCs (red dots) and aNSCs (blue dots) from the SVZ of adult mice as reported in a published microarray dataset [22] ($n=3$); *, adjusted p value < 0.05. **(C)** Box-and-whisker plots of *Dbx2* mRNA levels in freshly isolated qNSCs and aNSCs from the SVZ of adult mice as reported in a published RNA-seq dataset [18]. The lower and higher whiskers indicate the minimum and maximum values, respectively. The bottom and top of the box represent the first and third quartiles, respectively, and the band inside the box indicates the second quartile (the median). The + symbol indicates mean transcript levels. Red and blue triangles show individual experimental replicates for qNSCs and aNSCs, respectively ($n=4$); ***, $p<0.001$, Student's t-test. **(D)** Box-and-whisker plots of *Dbx2* mRNA levels in freshly isolated GFP high (GFP-H, red triangles) and GFP low (GFP-L, blue triangles) NSCs (largely corresponding to qNSCs and aNSCs, respectively) from the SVZ of adult mice as reported in a published RNA-seq dataset [15] ($n=4$); ***, adjusted p value < 0.001. **(E)** Box-and-whisker plots of *Dbx2* mRNA levels in adherent cultures of mouse young adult SVZ NSPCs that were treated for 6 h without exogenous growth factors (-GFs, red triangles), with 10 ng/ml FGF2 (orange triangles), with 20 ng/ml EGF (green triangles), or with EGF + FGF2 (E + F, blue triangles), followed by qRT-PCR analysis ($n=5$); *, $p<0.05$, one-way ANOVA. **(F)** Box-and-whisker plots of *Dbx2* mRNA levels in NSPC cultures that were treated for 8 h without exogenous growth factors (-GFs, red triangles), or were maintained for 6 h without growth factors and then treated for 2 h with 4, 20 or 100 ng/ml EGF (blue triangles), followed by qRT-PCR analysis ($n=4$); ***, $p<0.001$, one-way ANOVA. **(G)** Box-and-whisker plots of *Dbx2* mRNA levels, as detected by qRT-PCR, in NSPC cultures that were treated for 6 h without exogenous growth factors (-GFs, red triangles), with 20 ng/ml EGF (green triangles), or with 100 ng/ml TGFα (blue triangles), in the absence or in the presence of 2 μM AG1478 ($n=8$); *, $p<0.05$, **, $p<0.01$, one-way ANOVA. **(H)** Proposed model of *Dbx2* regulation in adult SVZ NSPCs. EGFR signaling inhibits *Dbx2* expression. EGFR signaling levels are reduced in qNSCs and in aged NSCs in comparison with aNSCs and adult NSCs (blue gradient), leading to increased *Dbx2* expression during NSC quiescence or aging (red gradient)

proliferation [30]. We speculated that *Dbx2* may promote cell cycle exit and entry in G0, or decrease the division rate of NSPCs remaining in the cell cycle. To test this hypotheses, we took advantage of previously described transgenic young adult NSPC lines with constitutive expression of either a mouse *Dbx2* transgene (*Dbx2*-NSPCs) or a control *GFP* transgene (*GFP*-NSPCs), and cultured them for 4–6 days (4-6 d) in non-adherent conditions to generate neurospheres [30]. We then used these cultures to quantify the percentage of *Dbx2*-NSPCs and *GFP*-NSPCs that were positive for Ki67, a nuclear marker expressed throughout the cell cycle, but not in cells that have exited the cell cycle. Moreover, we estimated the fraction of *Dbx2*-NSPCs and *GFP*-NSPCs in each phase of the cell cycle (G0/G1, S, G2/M) by flow cytometry quantification of DNA content in cells stained with PI. To make sure that the results were reproducible, we performed these analyses with two independent pairs of *Dbx2*-NSPC and *GFP*-NSPC lines [30]. Cell cycle exit of NSPCs in response to *Dbx2* overexpression would be expected to cause an increase in the fraction of cells in G0/G1 and a decrease of the fraction of Ki67+cells; however, these effects were not detectable in the *Dbx2*-NSPC lines as compared to *GFP*-NSPC cultures (Fig. 2A, D, E, H; Fig. S1A, D, E, H; Fig. S2A and D; representative images of Ki67-stained cultures are shown in Fig. 2I and J, and in Fig. S1I and J). Surprisingly, we detected a reproducible increase of the G2/M cell fraction upon *Dbx2* overexpression (Fig. 2C, D, H; Fig. S1C, D, H). To distinguish between cells in G2 and in M phases, we quantified the fraction of cells positive for pH3, a marker of cells undergoing mitosis. Mitotic histone H3 phosphorylation starts in pericentric heterochromatin in late G2, then spreads throughout the condensing chromatin during prophase, reaching a peak at metaphase; dephosphorylation of histone H3 begins in anaphase and ends in telophase [53]. In agreement with the dynamics of mitotic pH3 accumulation, we observed different patterns of pH3 immunostaining during NSPC progression through mitosis. Some of the pH3+NSPCs, likely corresponding to late G2 cells, showed a weaker staining in the form of isolated nuclear spots; during prophase, these pH3+foci increased in size and intensity, until the whole nucleus appeared to be stained (Fig. S3A to D). A peak in signal intensity was observed in NSPC nuclei between metaphase and early anaphase, followed by a progressive decrease between anaphase and telophase (Fig. S3I to L). We quantified

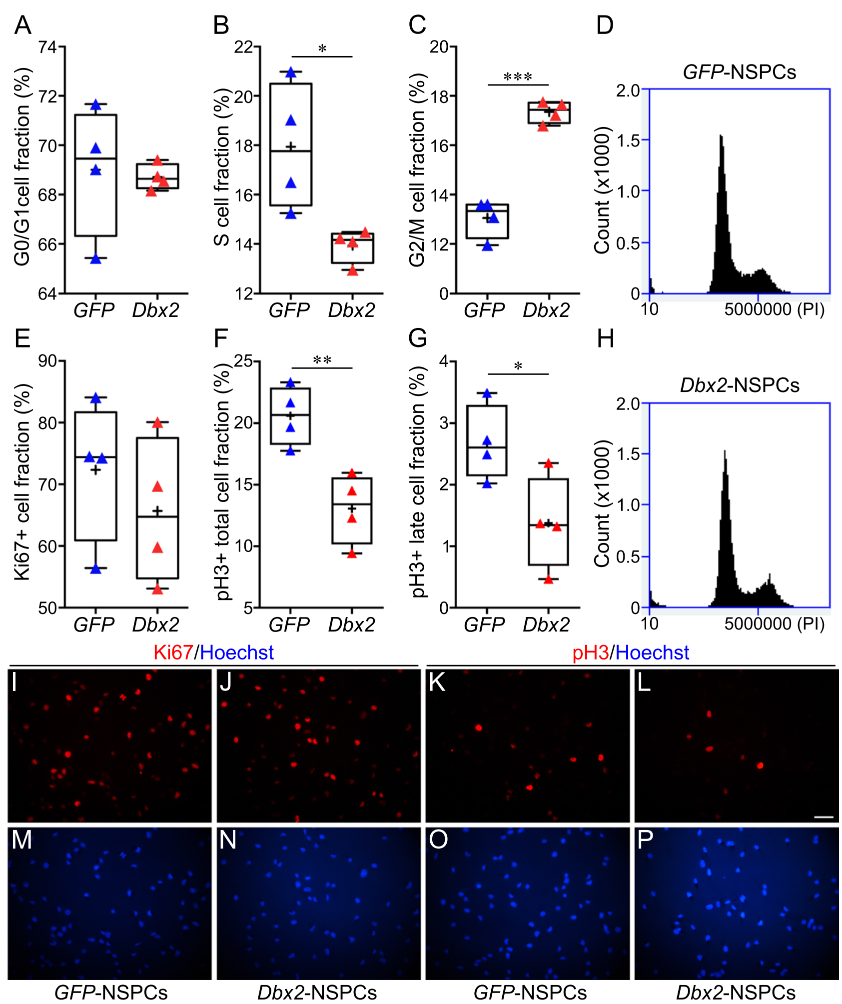

Fig. 2 Constitutive *Dbx2* overexpression inhibits the G2/M transition in young adult NSPCs. **(A to C)** Box-and-whisker plots of the fraction of *GFP*-NSPCs (blue triangles) and *Dbx2*-NSPCs (red triangles) in the G0/G1 **(A)**, S **(B)** and G2/M **(C)** phases of the cell cycle ($n=4$); *, $p<0.05$, ***, $p<0.001$, Student's t-test. The + symbols indicate mean percentages. Flow cytometry histograms of PI-stained *GFP*-NSPC and *Dbx2*-NSPC cultures from a representative experiment are shown in **(D)** and **(H)**, respectively. **(E to G)** Box-and-whisker plots of the fraction of Ki67+ **(E)**, pH3+ total **(F)** and pH3+ late **(G)** cells in *GFP*-NSPC (blue triangles) and *Dbx2*-NSPC (red triangles) cultures ($n=4$); *, $p<0.05$, **, $p<0.01$, Student's t-test. **(I to P)** Representative images of *GFP*-NSPC **(I, M, K, O)** and *Dbx2*-NSPC **(J, N, L, P)** cultures stained with anti-Ki67 **(I, J)** or anti-pH3 **(K, L)** antibodies. Hoechst nuclear staining is shown in **(M to P)**. Scale bar, 40 µm

the total percentage of pH3+NSPCs, which included all the cells engaging in the G2/M transition, as well as the percentage of NSPCs showing pH3 staining patterns typical of cells that have progressed beyond early prophase (Fig. S3D and I to L), which we named pH3+late cells. When compared with *GFP*-NSPCs, a decrease in the pH3+total cell fraction was detected in one of the *Dbx2*-NSPC lines, but not the other; however, both lines showed a reduction in the pH3+late cell fraction (Fig. 2F and G; Fig. S1F and G; Fig. S2B and E; representative images of pH3-stained cultures are shown in Fig. 2K and L, and in Fig S1K and L). The fraction of pH3+cells within the top 40% of the fluorescence intensity range, which likely include pH3+late cells, was also reduced in both *Dbx2*-NSPC lines (Fig. S1C and F). These results indicate that the accumulation in G2/M observed by flow

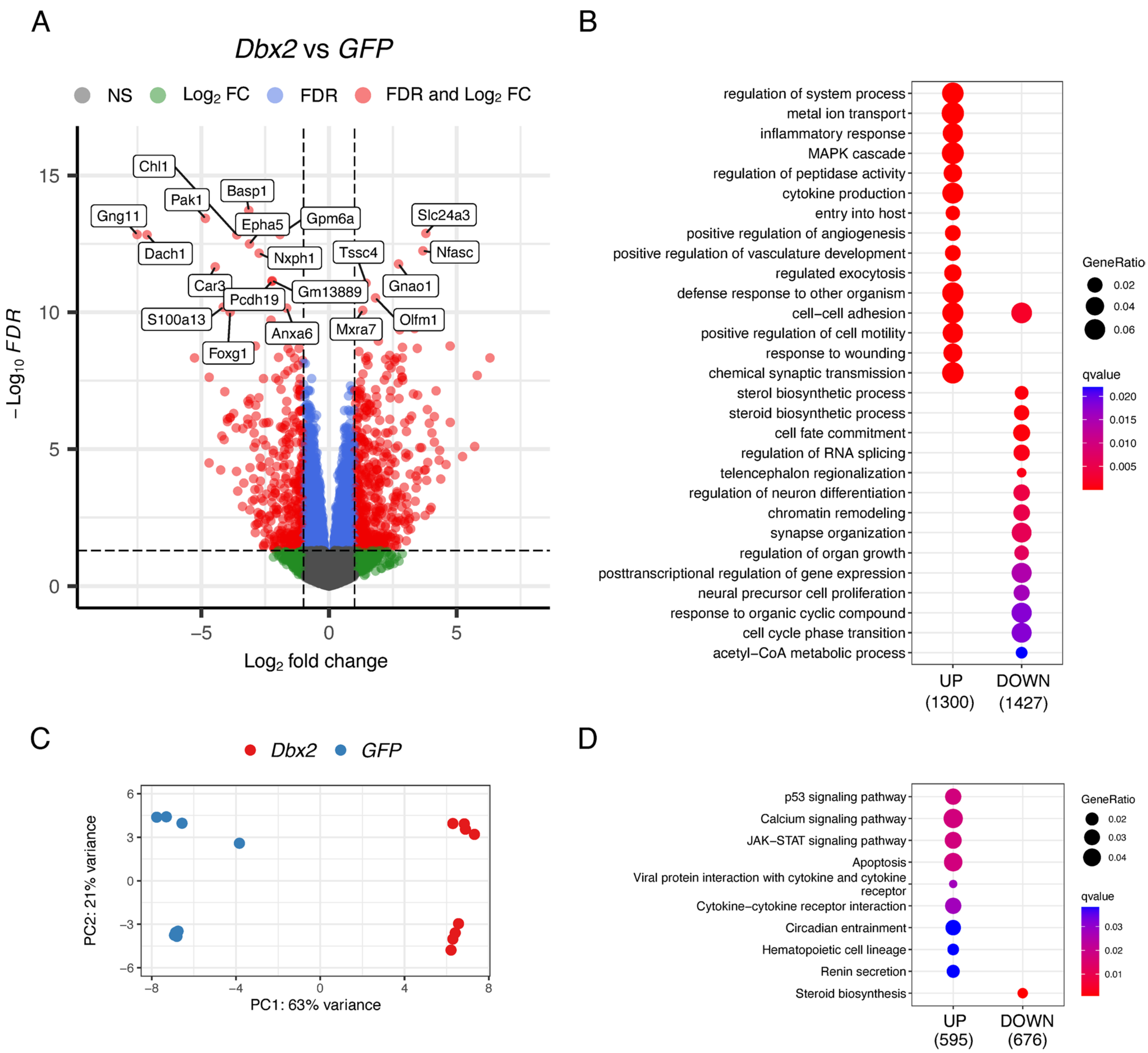

Fig. 3 Transcriptomic profiling of *Dbx2*-overexpressing NSPCs. **(A)** Volcano plot showing the distribution of -$\log_{10}$(FDR) values (Y axis) relative to $\log_2$(FC) values (X axis) resulting from the comparison of gene expression levels in *Dbx2*-NSPCs vs *GFP*-NSPCs. Red dots indicate DEGs associated with FDR < 0.05 and FC < -2 or FC > 2; blue dots indicate genes with FDR < 0.05 and -2 < FC < 2; green dots indicate genes with FC < -2 or FC > 2, and FDR > 0.05. Representative genes are highlighted in the plot. **(B)** Dot plot showing the GO terms enriched in the upregulated (left) and the downregulated (right) DEGs. The size of the dots is based on the count of the DEGs correlated with each term; the colour of the dots shows the qvalue associated with each term. **(C)** PCA plots showing that control experimental replicates (*GFP*-NSPCs, blue dots) and *Dbx2*-overexpressing experimental replicates (*Dbx2*-NSPCs, red dots) can be distinguished from each other along the PC1 axis. Control or *Dbx2*-overexpressing experimental replicates from independent cell lines carrying the same transgene can be distinguished along the PC2 axis. **(D)** Dot plot showing the KEGG pathways that are enriched in the upregulated (left) and the downregulated (right) DEGs

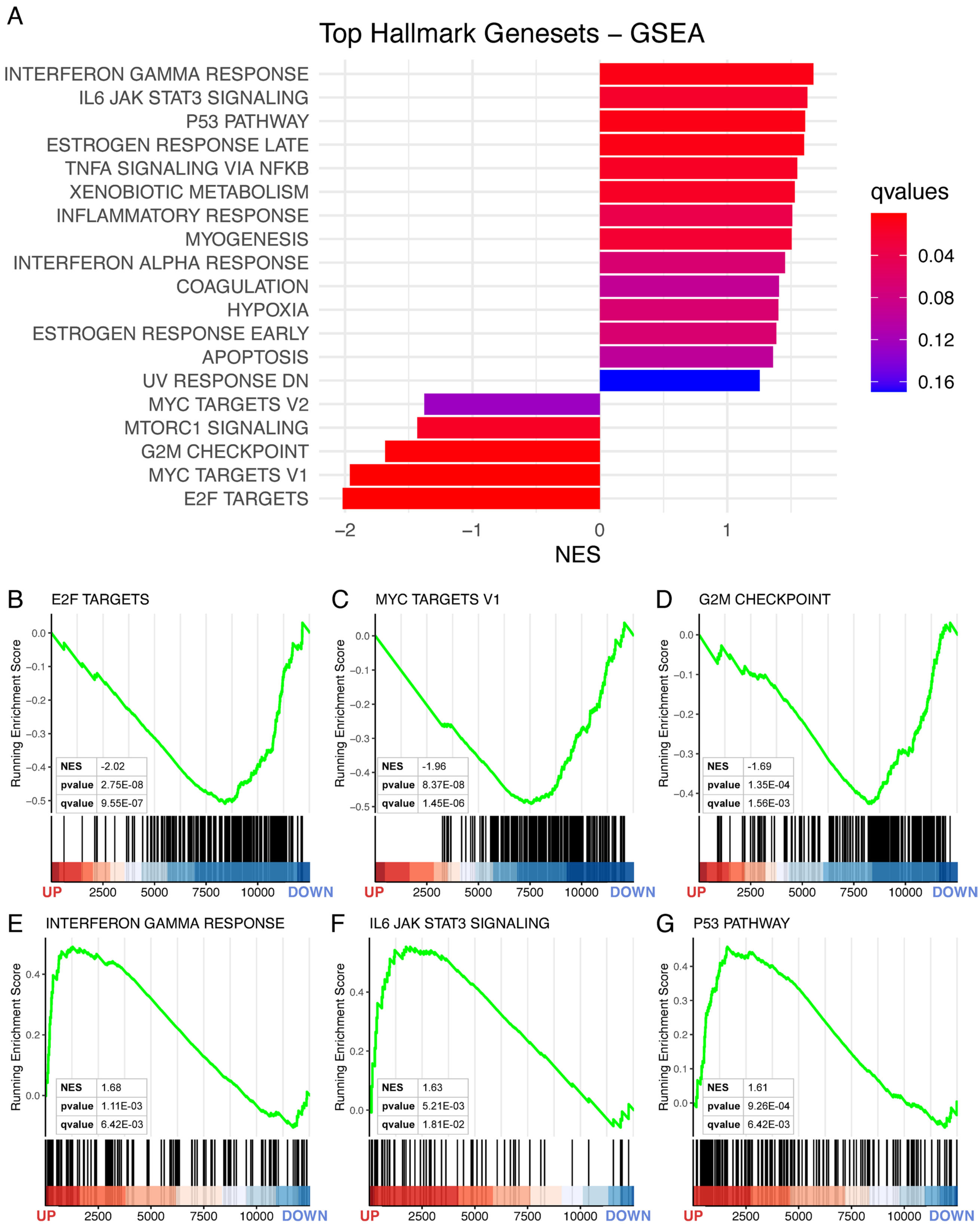
A
Top Hallmark Genesets – GSEA
INTERFERON GAMMA RESPONSE
IL6 JAK STAT3 SIGNALING
P53 PATHWAY
ESTROGEN RESPONSE LATE
TNFA SIGNALING VIA NFKB
XENOBIOTIC METABOLISM
INFLAMMATORY RESPONSE
MYOGENESIS
INTERFERON ALPHA RESPONSE
COAGULATION
HYPOXIA
ESTROGEN RESPONSE EARLY
APOPTOSIS
UV RESPONSE DN
MYC TARGETS V2
MTORC1 SIGNALING
G2M CHECKPOINT
MYC TARGETS V1
E2F TARGETS
NES
qvalues
B E2F TARGETS
NES -2.02
pvalue 2.75E-08
qvalue 9.55E-07
C MYC TARGETS V1
NES -1.96
pvalue 8.37E-08
qvalue 1.45E-06
D G2M CHECKPOINT
NES -1.69
pvalue 1.35E-04
qvalue 1.56E-03
E INTERFERON GAMMA RESPONSE
NES 1.68
pvalue 1.11E-03
qvalue 6.42E-03
F IL6 JAK STAT3 SIGNALING
NES 1.63
pvalue 5.21E-03
qvalue 1.81E-02
G P53 PATHWAY
NES 1.61
pvalue 9.26E-04
qvalue 6.42E-03
Running Enrichment Score
UP
DOWN

◂**Fig. 4** *Dbx2* overexpression affects the expression of gene sets related to cell cycle and inflammatory response. **(A)** Bar plot showing the top "Hallmark" gene sets correlated with the *Dbx2*-associated transcriptional signature (12533 genes), according to GSEA. The size and the colour of the bars indicate the NES value and the qvalue associated with each gene set, respectively. (**B** to **G**) Enrichment plots showing the top 3 NES < 0 gene sets (**B** to **D**), or the top 3 NES > 0 gene sets (**E** to **G**), in the *Dbx2*-associated signature. Vertical black lines indicate individual members of each gene set and their position within the ranked *Dbx2*-associated signature; the FC direction in *Dbx2*-overexpressing NSPCs is indicated in the X axis (down, FC < 0; up, FC > 0). The heat maps at the bottom of the plots highlight the proportion of *Dbx2*-downregulated genes (blue colour) and *Dbx2*-upregulated genes (red colour) in each gene set

cytometry is due to an altered mitotic progression in *Dbx2*-NSPC cultures. Therefore, they lead us to suggest that *Dbx2* negatively regulates the G2/M transition in NSPCs, hindering the progression through mitosis when its expression levels increase. The observation that one of the *Dbx2*-NSPC lines showed a weaker effect on the G2/M transition than the other is consistent with the comparatively weaker growth phenotype of the neurosphere cultures generated from this cell line [30], and might be explained by differences in the genetic or epigenetic background of the two cell lines, as suggested by PCA results (see below). Nonetheless, the number of cells undergoing cell division is decreased in both lines, which provides an explanation for the reduced size of the neurospheres formed by *Dbx2*-NSPCs.

Dbx2 Regulates NSPC Transcriptional Programmes Associated with Cell Cycle, Inflammatory Response and Lineage Progression

To gain insight into the molecular mechanisms mediating the effects of *Dbx2* overexpression in SVZ NSPCs, we performed a transcriptomic analysis with the transgenic NSPC lines used for cell cycle assays. To this aim, we performed RNA-seq and differential gene expression analysis with RNA samples obtained from 4-6 d non-adherent cultures of both lines of *Dbx2*-NSPCs and *GFP* NSPCs (4 independent experiments for each pair). PCA confirmed that the cell culture samples used for transcriptomic analysis were mainly clustered according to transgene expression (*Dbx2* or *GFP*) (PC1, 63% of variance), although samples belonging to the same experimental condition, but to independent cell lines, could also be distinguished (PC2, 21% of variance) (Fig. 3C). By setting a threshold of FDR < 0.05, we identified 2854 DEGs between *Dbx2*-NSPCs and *GFP*-NSCPs (1368 upregulated and 1486 downregulated genes in *Dbx2*-NSPCs) (Fig. 3A and Table S1).

We then performed GO enrichment analysis of the DEGs using the GO Biological Process database. As shown in Fig. 3B, the genes downregulated upon *Dbx2* overexpression were enriched for GO terms related to NSPC proliferation (e.g. "neural precursor cell proliferation", "cell cycle phase transition"), lineage progression (e.g. "cell fate commitment", "regulation of neuron differentiation"), and RNA processing (e.g. "regulation of RNA splicing"); the genes upregulated in *Dbx2*-overexpressing NSPCs were enriched for GO terms related to inflammatory response (e.g. "inflammatory response", "cytokine production"). DEG analysis using REACTOME and KEGG databases also indicated that pathways related to cell cycle and RNA processing were enriched in the downregulated genes, and pathways related to inflammatory response and cell cycle inhibition ("p53 signaling pathway") were enriched in the upregulated genes (Fig. 3D and Fig. S4).

To characterise these transcriptional effects in more detail, we analysed the transcriptome of *Dbx2*-overexpressing NSPCs by GSEA, a computational method that investigates the biological effects associated with a ranked gene list by determining whether the members of a gene set linked to a specific biological process tend to occur at the top or the bottom of the ranked gene list [46]. Since the size of the analysed gene list influences GSEA accuracy, we performed this analysis with a wider *Dbx2*-associated signature of 12533 genes, which included all the genes with detectable mRNA expression in *Dbx2*-NSPCs and GFP-NSPCs, irrespectively of FDR values. This gene list was ranked according to FC, followed by GSEA with "Hallmark" gene sets in MSigDB. Notably, several cell cycle-related gene sets ("E2F targets", "G2M checkpoint", "Myc targets") correlated with the *Dbx2*-associated signature (Fig. 4A), with negative NES values resulting from the enrichment of these gene sets among the genes downregulated in *Dbx2*-overexpressing NSPCs (Fig. 4B, C and D; Table S2). Moreover, several gene sets linked to inflammatory response (e.g. "Interferon gamma response", "IL6 JAK STAT3 signaling") or to cell cycle inhibition ("p53 pathway") correlated with the *Dbx2*-associated signature (Fig. 4A), with positive NES values resulting from the enrichment of these gene sets among the genes upregulated in *Dbx2*-overexpressing NSPCs (Fig. 4E, F and G, Table S2). Transcription factor motif enrichment analysis confirmed an enrichment of E2F and Myc motifs in the DEGs downregulated in *Dbx2*-overexpressing NSPCs, and an enrichment of p53 motifs in the upregulated DEGs (Fig. S5).

Given *Dbx2* effects on NSPC proliferation, we performed a more detailed analysis of the transcriptional changes related to cell cycle progression in *Dbx2*-overexpressing NSPCs. To this aim, we carried out GSEA using the *Dbx2*-associated signature and various gene sets related to different cell cycle phases as available in the "C2" curated gene sets collection in MSigDB. This analysis revealed a general negative correlation of the *Dbx2*-associated signature with cell cycle-related gene sets (Fig. S6). A characterization of the DEGs between *Dbx2*-NSPCs and *GFP*-NSCPs (FDR < 0.05) with KEGG cell cycle and p53 signaling pathway gene sets showed that several genes crucially implicated in the G1/S transition (*Cdk2*, *Cdk4*) or G2/M transition (*CycA*, *Cdk1*)

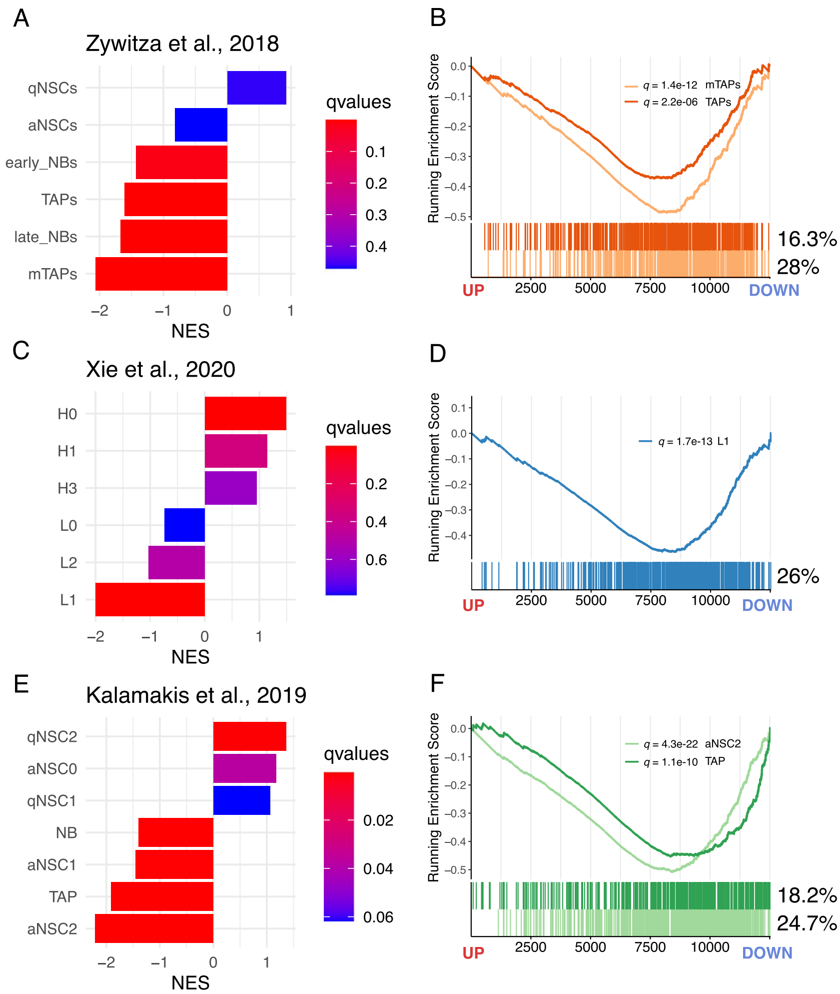

Fig. 5 *Dbx2* function is negatively correlated with neurogenic lineage progression. (**A**, **C** and **E**) Bar plots showing the correlation between the *Dbx2*-associated signature and the qNSC-specific, aNSC-specific, TAP-specific and NB-specific gene sets, as defined in recent studies [[47] (**A**), [15] (**C**), [14] (**E**)], according to GSEA. In (**C**), H0-H3 correspond to qNSC subpopulations, L0 to aNSCs, L1 to TAPs and L2 to NBs, as previously described [15]. (**B**, **D** and **F**) Enrichment plots showing selected cell type-specific gene sets in the *Dbx2*-associated signature. The percentages indicate the fraction of cell cycle genes in each gene set

were downregulated in *Dbx2*-overexpressing NSPCs, and key cell cycle inhibitors acting in the p53 pathway (*p21*, *Gadd45*) were upregulated (Fig. S7). These results suggest that elevated *Dbx2* expression broadly inhibits the transcriptional pathways involved in cell cycle progression.

The results of GSEA with cell cycle-related gene sets prompted us to use the same approach to investigate the effects of *Dbx2* overexpression on the transcriptional programmes associated with NSPC lineage progression. To this aim, we took advantage of the recently described single-cell transcriptomic signatures of qNSCs, aNSCs, TAPs and NBs of the adult mouse SVZ [14, 15, 47]; we then used the gene sets related to each of these cell populations to perform GSEA with the *Dbx2*-associated signature. Remarkably, the gene sets related to aNSCs, TAPs and NBs negatively correlated with the *Dbx2*-associated signature (Fig. 5, Table S3). Although the signature related to the whole qNSC population was not correlated with the *Dbx2*-associated signature (Fig. 5A), a positive correlation (NES > 0) was observed when the analysis was carried out using the gene sets related to specific qNSC subpopulations (Fig. 5C and E). Since aNSCs, TAPs and NBs encompass the proliferating NSPC pool of the SVZ neurogenic lineage, we wondered whether the negative correlation that we observed between the gene sets related to these cell populations and the *Dbx2*-associated signature may be driven by cell cycle-related genes. To address this question, we quantified the percentage of REACTOME and KEGG cell cycle genes among the aNSC-related and TAP-related gene sets. This quantification suggested that cell cycle genes alone did not explain the correlation between the aNSC/TAP-related and the *Dbx2*-associated signatures; for example, cell cycle genes accounted for only 26–28% of the genes in the signatures related to proliferative TAPs (mTAPs and L1) (Fig. 5B and D). We then filtered out cell cycle genes from aNSC/TAP signatures, selected the *Dbx2*-downregulated DEGs (FDR < 0.05) among the remaining genes, and performed GO enrichment analysis on the resulting gene lists. Notably, GO terms related to RNA processing (e.g. “RNA splicing”) prominently featured in all the analysed gene lists (Fig. 6). These data suggest that *Dbx2* may inhibit NSPC proliferation by regulating cell cycle-related genes, and NSPC lineage progression by modulating genes involved in RNA processing.

Fig. 6 *Dbx2* affects the expression of gene sets related to both RNA processing and neurogenic lineage progression. (**A**) Dot plot showing the GO terms enriched in the gene sets obtained by subtracting cell cycle genes, taken from the KEGG and REACTOME cell cycle gene sets, from the indicated NSPC signatures (TAPs and mTAPs, [47]; TAPs and aNSC2 [14]; L1 [15]), then selecting the downregulated DEGs in *Dbx2*-NSPCs vs *GFP*-NSPCs in the resulting gene lists. (**B**) Bar plot showing the FC of genes associated with the GO terms "RNA splicing, via transesterification reactions" and "mRNA splicing, via spliceosome", which are also associated with the NSPC signatures indicated in (**A**), and downregulated in *Dbx2*-NSPCs

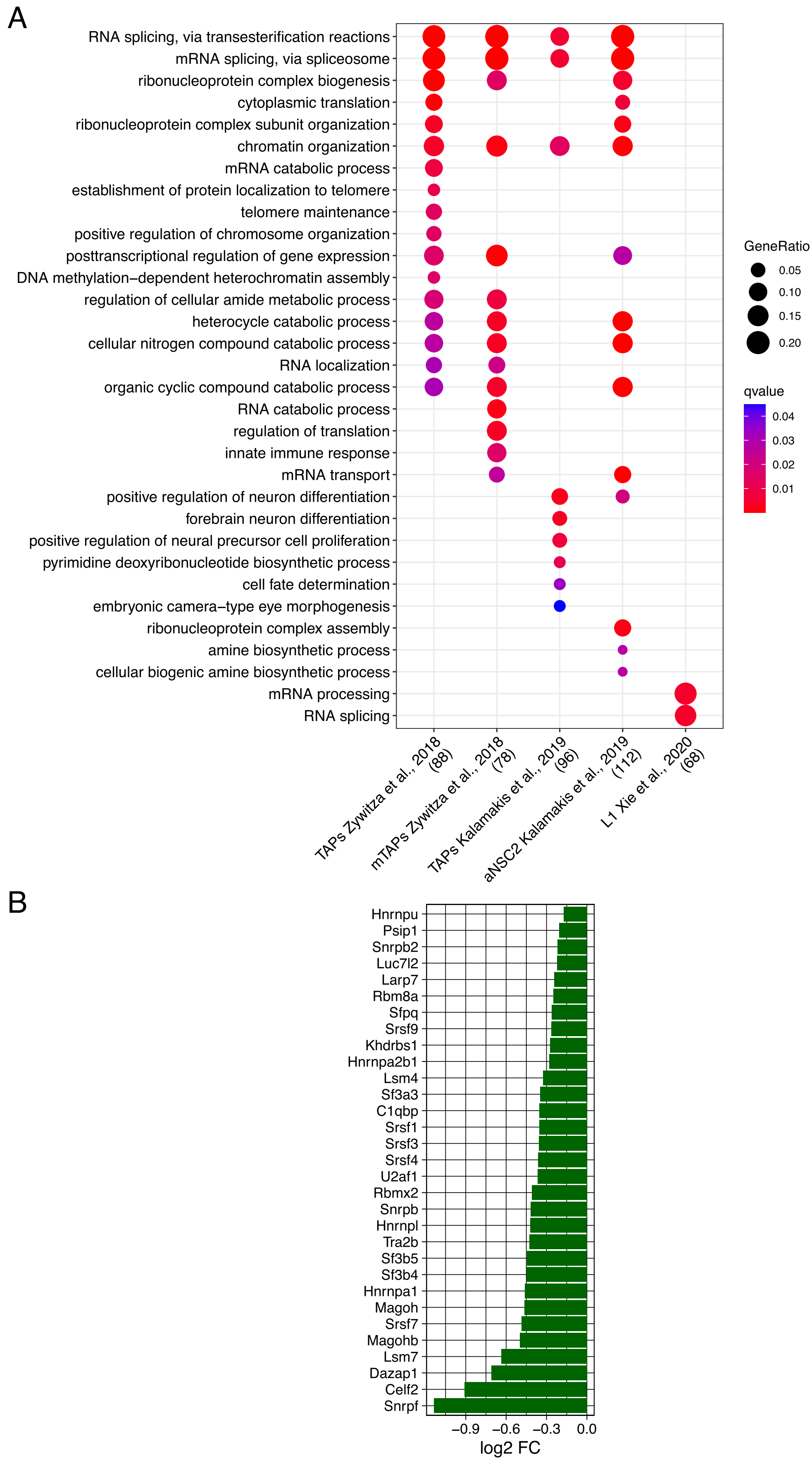

Discussion

In this study, we show that elevated *Dbx2* expression in NSPCs impairs the G2/M transition, causing accumulation in G2/M by hindering the progression through mitosis. Although we could not detect a clear effect of *Dbx2* overexpression on the G1/S transition, transcriptomic analyses revealed that *Dbx2* broadly regulates the cell cycle molecular networks, repressing genes implicated in cell cycle progression and activating genes involved in cell cycle arrest. Of note, signatures related to E2F, Myc and p53 were among the top hits, which is consistent with the recently described association between these factors and the transcriptomic profiles of aged NSPCs [15].

Recent studies suggest that the increase in the time spent by NSCs in a quiescent state, which is generally thought to be in G0, is a main driver of the neurogenic decline of aged mice [12–16]. Although *Drosophila* qNSCs can also be arrested in G2 [54], evidence that this may happen in mice is lacking. Transcriptomic comparison of qNSCs and aNSCs of the mouse SVZ, however, showed that both G1/S and G2/M signatures are downregulated in qNSCs [18]; thus, the inhibitory effects of *Dbx2* on the transcriptional networks associated with both the G1/S and G2/M transitions is compatible with a role in the increased quiescence of aged NSCs. Notably, the gene set downregulated upon *Dbx2* overexpression correlates with the transcriptomic signatures of the proliferative populations of the SVZ neurogenic lineage (aNSCs, TAPs and early NBs), supporting the implication of *Dbx2* in NSC quiescence from a different angle. The limited percentage of cell cycle genes contributing to this correlation suggests that it is not driven predominantly by cell cycle inhibition; furthermore, GO analysis indicates an additional negative effect of *Dbx2* on genes related to RNA processing. We speculate that increased *Dbx2* expression during SVZ aging may facilitate NSC progressing into quiescence by inhibiting cell cycle genes along with RNA processing genes.

Several categories associated with the inflammatory response were top hits among the genes upregulated by *Dbx2* overexpression. This is noteworthy, since inflammatory transcriptional signatures are associated with NSC quiescence, aged neurogenic niches and brain aging [8, 9, 18, 55]. We did not detect an increase in *Dbx2* expression levels in young adult NSPC cultures treated with IFNαγ, IL2/6 or TNFα (our unpublished observations); however, gene sets related to immune response (especially IFN signaling) were upregulated in SVZ NSPC cultures treated with BMP4 and FGF2 to induce quiescence [25]. Thus, these signatures may be activated in NSPCs independently of canonical cytokine-driven responses to regulate their proliferative state.

In conclusion, our study uncovers several links between increased *Dbx2* function and key features of NSPC aging. These include: i) the downregulation of gene networks implicated in cell cycle progression, the upregulation of those involved in cell cycle arrest and the inhibition of NSPC proliferation; ii) the upregulation of inflammatory response pathways; iii) the downregulation of the transcriptomic signatures of the proliferative neurogenic cell populations (aNSCs, TAPs and early NBs), which are depleted in the aged SVZ; iv) the negative regulation of *Dbx2* expression by EGFR signaling, which is reduced in the aged SVZ. This work has some limitations, since our functional experiments have been performed using *in vitro* NPSC cultures and gain-of-function approaches. Although some of the genes modulated upon *Dbx2* overexpression showed opposite changes in aged NSPC cultures expressing *Dbx2*-targeting shRNAs, this approach yielded a modest *Dbx2* knockdown in our hands [30]. Of note, *Dbx2* is a NSC-specific component of the recently reported molecular aging clocks in the mouse SVZ, and its age-associated modulation can be reversed by exercise [56], pointing to *Dbx2* as a potential biomarker of neurogenic niche aging and rejuvenation. By showing that *Dbx2* can promote age-associated changes in NSPC cultures, our *in vitro* analyses prompt the investigation of the functional role of *Dbx2* in the aging of *in vivo* neurogenic niches.

Supplementary Information The online version contains supplementary material available at https://doi.org/10.1007/s12015-023-10600-7.

Acknowledgements We thank Daniela Trisciuoglio and Paola Del Porto for help with the flow cytometry data shown in Fig. 2 and Fig. S1.

Author Contributions G.L. conceived the study and designed the experiments. A.G., P.S.N., S.D. and G.L. performed cell culture and sample preparation for endpoint analyses. A.G. and G.L performed qRT-PCR analysis. A.G., P.S.N. and S.D. performed immunofluorescence analysis. M.F. performed flow cytometry analysis. V.L. performed all the bioinformatic analysis. G.L. wrote the first manuscript draft. All authors contributed to data interpretation, critically revised the manuscript and approved its final version.

Funding Open access funding provided by Università degli Studi di Roma La Sapienza within the CRUI-CARE Agreement. This work was supported by research project grants from Sapienza University of Rome (calls 2017–2020; G.L., E.C., R.N.) and by the BBSRC (BBS/E/B/000C0421; P.J.R.-G.).

Data Availability RNA-seq data accompanying this paper are available through NCBI Gene Expression Omnibus (GEO) repository, under accession number GSE222691.

Declarations

Ethics Approval The original derivation of mouse SVZ NSPCs was performed in accordance with EU and Italian regulations and with ethical approval by the Ethical Committee for Animal Research of the Italian Ministry of Health, as described [30]. No additional animals were employed for the experiments reported in the present study.

Competing Interest The authors have no relevant financial or non-financial interests to disclose.

References

1. Quaresima, S., Istiaq, A., Jono, H., Cacci, E., Ohta, K., & Lupo, G. (2022). Assessing the role of ependymal and vascular cells as sources of extracellular cues regulating the mouse ventricular-subventricular zone neurogenic niche. *Frontiers in Cell and Developmental Biology, 10*, 845567. https://doi.org/10.3389/fcell.2022.845567
2. Lim, D. A., & Alvarez-Buylla, A. (2016). The adult Ventricular-Subventricular Zone (V-SVZ) and Olfactory Bulb (OB) neurogenesis. *Cold Spring Harbor Perspectives in Biology, 8*(5), a018820. https://doi.org/10.1101/cshperspect.a018820
3. Kempermann, G., Song, H., & Gage, F. H. (2015). Neurogenesis in the adult hippocampus. *Cold Spring Harbor Perspectives in Biology, 7*(9), a018812. https://doi.org/10.1101/cshperspect.a018812
4. Urbán, N., Blomfield, I. M., & Guillemot, F. (2019). Quiescence of adult mammalian neural stem cells: A highly regulated rest. *Neuron, 104*(5), 834–848. https://doi.org/10.1016/j.neuron.2019.09.026
5. Obernier, K., & Alvarez-Buylla, A. (2019). Neural stem cells: origin, heterogeneity and regulation in the adult mammalian brain. *Development (Cambridge, England), 146*(4), dev156059. https://doi.org/10.1242/dev.156059
6. Terreros-Roncal, J., Moreno-Jiménez, E. P., Flor-García, M., Rodríguez-Moreno, C. B., Trinchero, M. F., Cafini, F., …, & Llorens-Martín, M. (2021). Impact of neurodegenerative diseases on human adult hippocampal neurogenesis. *Science (New York, N.Y.), 374*(6571), 1106–1113. https://doi.org/10.1126/science.abl5163
7. Moreno-Jiménez, E. P., Flor-García, M., Terreros-Roncal, J., Rábano, A., Cafini, F., Pallas-Bazarra, N., …, & Llorens-Martín, M. (2019). Adult hippocampal neurogenesis is abundant in neurologically healthy subjects and drops sharply in patients with Alzheimer's disease. *Nature Medicine*, *25*(4), 554–560. https://doi.org/10.1038/s41591-019-0375-9
8. Navarro Negredo, P., Yeo, R. W., & Brunet, A. (2020). Aging and rejuvenation of neural stem cells and their niches. *Cell Stem Cell, 27*(2), 202–223. https://doi.org/10.1016/j.stem.2020.07.002
9. Lupo, G., Gioia, R., Nisi, P. S., Biagioni, S., & Cacci, E. (2019). Molecular mechanisms of neurogenic aging in the adult mouse subventricular zone. *Journal of Experimental Neuroscience, 13*, 1179069519829040. https://doi.org/10.1177/1179069519829040
10. Calzolari, F., Michel, J., Baumgart, E. V., Theis, F., Götz, M., & Ninkovic, J. (2015). Fast clonal expansion and limited neural stem cell self-renewal in the adult subependymal zone. *Nature Neuroscience, 18*(4), 490–492. https://doi.org/10.1038/nn.3963
11. Encinas, J. M., Michurina, T. V., Peunova, N., Park, J.-H., Tordo, J., Peterson, D. A., …, & Enikolopov, G. (2011). Division-coupled astrocytic differentiation and age-related depletion of neural stem cells in the adult hippocampus. *Cell Stem Cell*, *8*(5), 566–579. https://doi.org/10.1016/j.stem.2011.03.010
12. Ibrayeva, A., Bay, M., Pu, E., Jörg, D. J., Peng, L., Jun, H., … Bonaguidi, M. A. (2021). Early stem cell aging in the mature brain. *Cell Stem Cell*, *28*(5), 955–966.e7. https://doi.org/10.1016/j.stem.2021.03.018
13. Bast, L., Calzolari, F., Strasser, M. K., Hasenauer, J., Theis, F. J., Ninkovic, J., & Marr, C. (2018). Increasing neural stem cell division asymmetry and quiescence are predicted to contribute to the age-related decline in neurogenesis. *Cell Reports, 25*(12), 3231-3240.e8. https://doi.org/10.1016/j.celrep.2018.11.088
14. Kalamakis, G., Brüne, D., Ravichandran, S., Bolz, J., Fan, W., Ziebell, F., …, & Martin-Villalba, A. (2019). Quiescence modulates stem cell maintenance and regenerative capacity in the aging brain. *Cell*, *176*(6), 1407–1419.e14. https://doi.org/10.1016/j.cell.2019.01.040
15. Xie, X. P., Laks, D. R., Sun, D., Poran, A., Laughney, A. M., Wang, Z., …, & Parada, L. F. (2020). High-resolution mouse subventricular zone stem-cell niche transcriptome reveals features of lineage, anatomy, and aging. *Proceedings of the National Academy of Sciences of the United States of America*, *117*(49), 31448–31458. https://doi.org/10.1073/pnas.2014389117
16. Harris, L., Rigo, P., Stiehl, T., Gaber, Z. B., Austin, S. H. L., Masdeu, M. D. M., …, & Guillemot, F. (2021). Coordinated changes in cellular behavior ensure the lifelong maintenance of the hippocampal stem cell population. *Cell Stem Cell*, *28*(5), 863–876.e6. https://doi.org/10.1016/j.stem.2021.01.003
17. Basak, O., Krieger, T. G., Muraro, M. J., Wiebrands, K., Stange, D. E., Frias-Aldeguer, J., …, & Clevers, H. (2018). Troy+ brain stem cells cycle through quiescence and regulate their number by sensing niche occupancy. *Proceedings of the National Academy of Sciences of the United States of America*, *115*(4), E610–E619. https://doi.org/10.1073/pnas.1715911114
18. Belenguer, G., Duart-Abadia, P., Jordán-Pla, A., Domingo-Muelas, A., Blasco-Chamarro, L., Ferrón, S. R., …, & Fariñas, I. (2021). Adult neural stem cells are alerted by systemic inflammation through TNF-α receptor signaling. *Cell Stem Cell*, *28*(2), 285–299.e9. https://doi.org/10.1016/j.stem.2020.10.016
19. Apostolopoulou, M., Kiehl, T. R., Winter, M., Cardenas De La Hoz, E., Boles, N. C., Bjornsson, C. S., …, & Temple, S. (2017). Non-monotonic changes in progenitor cell behavior and gene expression during aging of the adult V-SVZ neural stem cell niche. *Stem Cell Reports*, *9*(6), 1931–1947. https://doi.org/10.1016/j.stemcr.2017.10.005
20. Cochard, L. M., Levros, L.-C., Joppé, S. E., Pratesi, F., Aumont, A., & Fernandes, K. J. L. (2021). Manipulation of EGFR-induced signaling for the recruitment of quiescent neural stem cells in the adult mouse forebrain. *Frontiers in Neuroscience, 15*, 621076. https://doi.org/10.3389/fnins.2021.621076
21. Enwere, E., Shingo, T., Gregg, C., Fujikawa, H., Ohta, S., & Weiss, S. (2004). Aging results in reduced epidermal growth factor receptor signaling, diminished olfactory neurogenesis, and deficits in fine olfactory discrimination. *The Journal of Neuroscience: The Official Journal of the Society for Neuroscience, 24*(38), 8354–8365. https://doi.org/10.1523/JNEUROSCI.2751-04.2004
22. Codega, P., Silva-Vargas, V., Paul, A., Maldonado-Soto, A. R., Deleo, A. M., Pastrana, E., & Doetsch, F. (2014). Prospective identification and purification of quiescent adult neural stem cells from their in vivo niche. *Neuron, 82*(3), 545–559. https://doi.org/10.1016/j.neuron.2014.02.039
23. Kobayashi, T., Piao, W., Takamura, T., Kori, H., Miyachi, H., Kitano, S., …, & Kageyama, R. (2019). Enhanced lysosomal degradation maintains the quiescent state of neural stem cells. *Nature Communications*, *10*(1), 5446. https://doi.org/10.1038/s41467-019-13203-4

24. Dulken, B. W., Buckley, M. T., Navarro Negredo, P., Saligrama, N., Cayrol, R., Leeman, D. S., …, & Brunet, A. (2019). Single-cell analysis reveals T cell infiltration in old neurogenic niches. *Nature*, *571*(7764), 205–210. https://doi.org/10.1038/s41586-019-1362-5
25. Marqués-Torrejón, M. Á., Williams, C. A. C., Southgate, B., Alfazema, N., Clements, M. P., Garcia-Diaz, C., …, & Pollard, S. M. (2021). LRIG1 is a gatekeeper to exit from quiescence in adult neural stem cells. *Nature Communications*, *12*(1), 2594. https://doi.org/10.1038/s41467-021-22813-w
26. Pineda, J. R., Daynac, M., Chicheportiche, A., Cebrian-Silla, A., Sii Felice, K., Garcia-Verdugo, J. M., …, & Mouthon, M.-A. (2013). Vascular-derived TGF-β increases in the stem cell niche and perturbs neurogenesis during aging and following irradiation in the adult mouse brain. *EMBO molecular medicine*, *5*(4), 548–562. https://doi.org/10.1002/emmm.201202197
27. Yamada, T., Kerever, A., Yoshimura, Y., Suzuki, Y., Nonaka, R., Higashi, K., …, & Arikawa-Hirasawa, E. (2017). Heparan sulfate alterations in extracellular matrix structures and fibroblast growth factor-2 signaling impairment in the aged neurogenic niche. *Journal of Neurochemistry*, *142*(4), 534–544. https://doi.org/10.1111/jnc.14081
28. Shi, Z., Geng, Y., Liu, J., Zhang, H., Zhou, L., Lin, Q., …, & Sun, Y. E. (2018). Single-cell transcriptomics reveals gene signatures and alterations associated with aging in distinct neural stem/progenitor cell subpopulations. *Protein & Cell*, *9*(4), 351–364. https://doi.org/10.1007/s13238-017-0450-2
29. Leeman, D. S., Hebestreit, K., Ruetz, T., Webb, A. E., McKay, A., Pollina, E. A., …, & Brunet, A. (2018). Lysosome activation clears aggregates and enhances quiescent neural stem cell activation during aging. *Science (New York, N.Y.)*, *359*(6381), 1277–1283. https://doi.org/10.1126/science.aag3048
30. Lupo, G., Nisi, P. S., Esteve, P., Paul, Y.-L., Novo, C. L., Sidders, B., …, & Rugg-Gunn, P. J. (2018). Molecular profiling of aged neural progenitors identifies Dbx2 as a candidate regulator of age-associated neurogenic decline. *Aging Cell*, *17*(3), e12745. https://doi.org/10.1111/acel.12745
31. Pierani, A., Brenner-Morton, S., Chiang, C., & Jessell, T. M. (1999). A sonic hedgehog-independent, retinoid-activated pathway of neurogenesis in the ventral spinal cord. *Cell, 97*(7), 903–915. https://doi.org/10.1016/s0092-8674(00)80802-8
32. Shoji, H., Ito, T., Wakamatsu, Y., Hayasaka, N., Ohsaki, K., Oyanagi, M., …, & Takahashi, N. (1996). Regionalized expression of the Dbx family homeobox genes in the embryonic CNS of the mouse. *Mechanisms of Development*, *56*(1–2), 25–39. https://doi.org/10.1016/0925-4773(96)00509-6
33. Carucci, N., Cacci, E., Nisi, P. S., Licursi, V., Paul, Y.-L., Biagioni, S., …, & Lupo, G. (2017). Transcriptional response of Hoxb genes to retinoid signalling is regionally restricted along the neural tube rostrocaudal axis. *Royal Society Open Science*, *4*(4), 160913. https://doi.org/10.1098/rsos.160913
34. Soldati, C., Cacci, E., Biagioni, S., Carucci, N., Lupo, G., Perrone-Capano, C., …, & Augusti-Tocco, G. (2012). Restriction of neural precursor ability to respond to Nurr1 by early regional specification. *PloS One*, *7*(12), e51798. https://doi.org/10.1371/journal.pone.0051798
35. Licursi, V., Anzellotti, S., Favaro, J., Sineri, S., Carucci, N., Cundari, E., …, & Negri, R. (2020). X-ray irradiated cultures of mouse cortical neural stem/progenitor cells recover cell viability and proliferation with dose-dependent kinetics. *Scientific Reports*, *10*(1), 6562. https://doi.org/10.1038/s41598-020-63348-2
36. Schneider, C. A., Rasband, W. S., & Eliceiri, K. W. (2012). NIH image to ImageJ: 25 years of image analysis. *Nature Methods, 9*(7), 671–675. https://doi.org/10.1038/nmeth.2089
37. Lunde, A., & Glover, J. C. (2020). A versatile toolbox for semi-automatic cell-by-cell object-based colocalization analysis. *Scientific Reports, 10*(1), 19027. https://doi.org/10.1038/s41598-020-75835-7
38. Dobin, A., Davis, C. A., Schlesinger, F., Drenkow, J., Zaleski, C., Jha, S., …, & Gingeras, T. R. (2013). STAR: ultrafast universal RNA-seq aligner. *Bioinformatics (Oxford, England)*, *29*(1), 15–21. https://doi.org/10.1093/bioinformatics/bts635
39. Robinson, M. D., McCarthy, D. J., & Smyth, G. K. (2010). edgeR: A Bioconductor package for differential expression analysis of digital gene expression data. *Bioinformatics (Oxford, England), 26*(1), 139–140. https://doi.org/10.1093/bioinformatics/btp616
40. Huber, W., Carey, V. J., Gentleman, R., Anders, S., Carlson, M., Carvalho, B. S., …, & Morgan, M. (2015). Orchestrating high-throughput genomic analysis with Bioconductor. *Nature Methods*, *12*(2), 115–121. https://doi.org/10.1038/nmeth.3252
41. Gentleman, R. C., Carey, V. J., Bates, D. M., Bolstad, B., Dettling, M., Dudoit, S., …, & Zhang, J. (2004). Bioconductor: open software development for computational biology and bioinformatics. *Genome Biology*, *5*(10), R80. https://doi.org/10.1186/gb-2004-5-10-r80
42. Wu, T., Hu, E., Xu, S., Chen, M., Guo, P., Dai, Z., …, & Yu, G. (2021). clusterProfiler 4.0: A universal enrichment tool for interpreting omics data. *Innovation (New York, N.Y.)*, *2*(3), 100141. https://doi.org/10.1016/j.xinn.2021.100141
43. Ashburner, M., Ball, C. A., Blake, J. A., Botstein, D., Butler, H., Cherry, J. M., …, & Sherlock, G. (2000). Gene ontology: tool for the unification of biology. The Gene Ontology Consortium. *Nature Genetics*, *25*(1), 25–29. https://doi.org/10.1038/75556
44. Croft, D., Mundo, A. F., Haw, R., Milacic, M., Weiser, J., Wu, G., …, & D'Eustachio, P. (2014). The reactome pathway knowledgebase. *Nucleic Acids Research*, *42*(Database issue), D472–477. https://doi.org/10.1093/nar/gkt1102
45. Ogata, H., Goto, S., Sato, K., Fujibuchi, W., Bono, H., & Kanehisa, M. (1999). KEGG: Kyoto encyclopedia of genes and genomes. *Nucleic Acids Research, 27*(1), 29–34. https://doi.org/10.1093/nar/27.1.29
46. Subramanian, A., Tamayo, P., Mootha, V. K., Mukherjee, S., Ebert, B. L., Gillette, M. A., …, & Mesirov, J. P. (2005). Gene set enrichment analysis: A knowledge-based approach for interpreting genome-wide expression profiles. *Proceedings of the National Academy of Sciences of the United States of America*, *102*(43), 15545–15550. https://doi.org/10.1073/pnas.0506580102
47. Zywitza, V., Misios, A., Bunatyan, L., Willnow, T. E., & Rajewsky, N. (2018). Single-cell transcriptomics characterizes cell types in the subventricular zone and uncovers molecular defects impairing adult neurogenesis. *Cell Reports, 25*(9), 2457-2469.e8. https://doi.org/10.1016/j.celrep.2018.11.003
48. Kuleshov, M. V., Jones, M. R., Rouillard, A. D., Fernandez, N. F., Duan, Q., Wang, Z., …, & Ma'ayan, A. (2016). Enrichr: a comprehensive gene set enrichment analysis web server 2016 update. *Nucleic Acids Research*, *44*(W1), W90–97. https://doi.org/10.1093/nar/gkw377
49. Castro-Mondragon, J. A., Riudavets-Puig, R., Rauluseviciute, I., Lemma, R. B., Turchi, L., Blanc-Mathieu, R., …, & Mathelier, A. (2022). JASPAR 2022: the 9th release of the open-access database of transcription factor binding profiles. *Nucleic Acids Research*, *50*(D1), D165–D173. https://doi.org/10.1093/nar/gkab1113
50. Han, H., Cho, J.-W., Lee, S., Yun, A., Kim, H., Bae, D., …, & Lee, I. (2018). TRRUST v2: an expanded reference database of human and mouse transcriptional regulatory interactions. *Nucleic Acids Research*, *46*(D1), D380–D386. https://doi.org/10.1093/nar/gkx1013
51. ENCODE Project Consortium, Moore, J. E., Purcaro, M. J., Pratt, H. E., Epstein, C. B., Shoresh, N., …, & Weng, Z. (2020).

Expanded encyclopaedias of DNA elements in the human and mouse genomes. *Nature*, *583*(7818), 699–710. https://doi.org/10.1038/s41586-020-2493-4
52. Lachmann, A., Xu, H., Krishnan, J., Berger, S. I., Mazloom, A. R., & Ma'ayan, A. (2010). ChEA: Transcription factor regulation inferred from integrating genome-wide ChIP-X experiments. *Bioinformatics (Oxford, England), 26*(19), 2438–2444. https://doi.org/10.1093/bioinformatics/btq466
53. Hendzel, M. J., Wei, Y., Mancini, M. A., Van Hooser, A., Ranalli, T., Brinkley, B. R., …, & Allis, C. D. (1997). Mitosis-specific phosphorylation of histone H3 initiates primarily within pericentromeric heterochromatin during G2 and spreads in an ordered fashion coincident with mitotic chromosome condensation. *Chromosoma*, *106*(6), 348–360. https://doi.org/10.1007/s004120050256
54. Otsuki, L., & Brand, A. H. (2018). Cell cycle heterogeneity directs the timing of neural stem cell activation from quiescence. *Science (New York, N.Y.), 360*(6384), 99–102. https://doi.org/10.1126/science.aan8795
55 Lupo, G., Gaetani, S., Cacci, E., Biagioni, S., & Negri, R. (2019). Molecular signatures of the aging brain: Finding the links between genes and phenotypes. *Neurotherapeutics: The Journal of the American Society for Experimental NeuroTherapeutics, 16*(3), 543–553. https://doi.org/10.1007/s13311-019-00743-2
56. Buckley, M. T., Sun, E. D., George, B. M., Liu, L., Schaum, N., Xu, L., …, & Brunet, A. (2022). Cell-type-specific aging clocks to quantify aging and rejuvenation in neurogenic regions of the brain. *Nature Aging*, 1–17. https://doi.org/10.1038/s43587-022-00335-4

Publisher's Note Springer Nature remains neutral with regard to jurisdictional claims in published maps and institutional affiliations.